Eur Radiol (2002) 12:1962–1970
DOI 10.1007/s00330-002-1379-1

Hans-Ulrich Kauczor
Alexander Hanke
Edwin J.R. van Beek

Assessment of lung ventilation by MR imaging: current status and future perspectives

Received: 22 January 2002
Accepted: 23 January 2002
Published online: 24 May 2002

H.-U. Kauczor (✉) · A. Hanke
Klinik für Radiologie,
Johannes Gutenberg-Universität Mainz,
Langenbeckstrasse 1, 55131 Mainz,
Germany
e-mail:
kauczor@radiologie.klinik.uni-mainz.de
Tel.: +49-6131-176783
Fax: +49-6131-176633

E.J.R. van Beek
Unit of Academic Radiology,
Royal Hallamshire Hospital,
Glossop Road, Sheffield S10 2JF, UK

Abstract The aim of this paper is to review the present status of novel MRI techniques as a new important instrument for functional ventilation imaging. The current status and future perspectives in research and clinical applications are summarized. Morphological lung imaging is based on chest radiography and computed tomography, whereas scintigraphy is used for ventilation imaging. During recent years, MRI has emerged as a new means for functional imaging of ventilation. Aerosolized contrast agents and oxygen are used in proton imaging, whereas non-proton imaging relies on fluorine compounds, such as sulfur hexafluoride and perfluorcarbons, or on hyperpolarized noble gases, such as helium-3 or xenon-129. All the gases are administered as inhaled "contrast agents" for imaging of the airways and airspaces. In general, straightforward images demonstrate the homogeneity of ventilation in a breath-hold and allow for determination of ventilated lung. The different properties of the different compounds enable the measurement of additional functional parameters. They comprise airspace size, regional oxygen partial pressure, and analysis of ventilation distribution, ventilation/perfusion ratios, and gas exchange, including oxygen uptake. Novel MRI techniques provide the potential for functional imaging of ventilation. The next steps include definition of the value and the potential of the different contrast mechanisms as well as determination of the significance of the functional information with regard to physiological research and patient management in chronic obstructive pulmonary disease and others.

Keywords Lung · MR · Contrast enhancement · Hyperpolarized inert gases

Introduction

Imaging of the lung may consist of anatomical (parenchymal) imaging and functional imaging. At present, routine clinical imaging of the lung parenchyma is performed using chest radiography and CT. Computed tomography is the gold standard imaging modality for the morphological assessment of the pulmonary parenchyma with high spatial resolution (slice thickness as low as 1 mm). Dedicated strategies are applied to estimate lung function [1]. By using paired inspiratory and expiratory scans, hypoventilated lung areas caused by expiratory obstruction, i.e., air trapping, can be detected [2]. In addition, dynamic CT (spiral CT without table movement) is feasible. A temporal resolution of 100 ms can be reached [3]; however, this approach is limited to one slice. Larger coverage can be achieved by the use of multislice CT. The whole lung can be scanned within 5 s. This temporal resolution is not suited to derive functional parameters. Attempts of direct visualization of ventilation using CT consist of xenon-enhanced CT and the use of an aerosolized contrast agent. Both techniques aim at an increase of lung density reflecting regional ventilation. The increase in density is small and further postpro-

cessing is required [4, 5]; thus, the use of CT for functional assessment of ventilation is quite limited.

In general, nuclear medicine techniques are widely used to visualize pulmonary perfusion and ventilation. They are regarded as the gold standard for functional imaging studies. Gaseous compounds have the advantage of greater ease of distribution into the smaller airways, whereas aerosols are more prone to central deposition [6]. Major drawbacks are the limitation in spatial and temporal resolution. Improved anatomical detail is offered with the use of single photon emission CT, but this has a negative effect on temporal resolution [7]. More sophisticated techniques rely on positron emission tomography. It allows for an in-plane resolution of ~10 mm and a temporal resolution in the range of 30 s; however, the potential of broad clinical use appears limited, since the technical requirements are very demanding [8].

In comparison with the techniques described above, MRI does not rely on ionizing radiation, and offers new strategies for the functional assessment of ventilation with high spatial and/or temporal resolution [9]. The aim of this article is to update the knowledge of these emerging techniques and their scientific and clinical applications considering new image-derived functional parameters, such as pulmonary microstructure, regional oxygen partial pressure, regional oxygen uptake, and ventilation/perfusion ratios.

The straightforward application of T1- or T2-weighted proton MRI is significantly hampered by the low concentration of spins within the lung, significant susceptible artifacts, as well as cardiac and respiratory motion. Considering these challenges, ways to increase the signal-to-noise ratio (SNR) and new contrast mechanisms are a field of ongoing research.

Administration of aerosolized contrast agents

Aerosolization of gadolinium chelates and administration by inhalation seems trivial and was investigated in the 1980s [10]. Different formulations were used and multiple animal experiments performed [11]. Although administration of gadolinium chelates elicited a relatively homogeneous enhancement of the lung, the maximum of signal intensity obtained was low (approximate mean increase 120%; Fig. 1) [11, 12]. The mean particle size of the nebulized aerosol was 2.5 µm. Furthermore, aerosols have the same problem as scintigraphy in that central deposition occurs in patients with airways diseases. Dynamic imaging of ventilation is not possible because of the long administration time of 10 min or longer [12]. Investigations in humans are still pending.

Fig. 1 Hydrogen-1 MRI (coronal subtraction) in a pig following 20 min of mechanical aerosol delivery showing homogeneous Gd-DTPA distribution. (Courtesy of P. Haage)

Oxygen enhancement

The use of oxygen as a contrast agent for MRI of ventilation was first proposed in 1996 [13]. Although molecular oxygen is weakly paramagnetic, its effect in the lung is significant due to the enormous surface area of the lung and the large difference in oxygen partial pressure between breathing room air (20% oxygen) and pure oxygen. The signal changes in the lung are explained by T1-shortening in lung tissue and blood due to the paramagnetic properties of dissolved molecular oxygen. After subtraction of T1-weighted inversion recovery images (HASTE or RARE) obtained while breathing room air from images obtained after breathing 100% oxygen, images display the distribution of molecular oxygen within lung parenchyma and veins with a typical increase in signal intensity of the order of 15% [14]. By means of varying the inversion time images can be weighted for ventilation or perfusion. Image quality is improved by suppression of the background signal [15]. In combina-

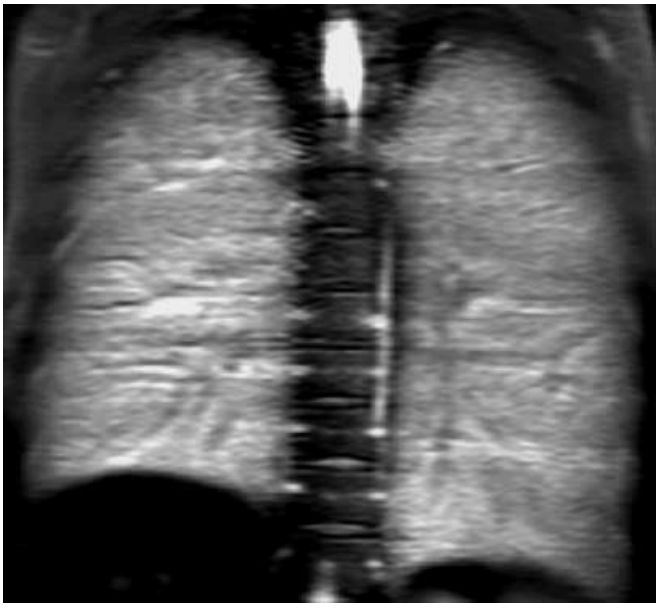

Fig. 2 Hydrogen-1 MRI with oxygen enhancement in a healthy volunteer showing homogeneous ventilation and enhancement of pulmonary veins reflecting the distribution of dissolved molecular oxygen

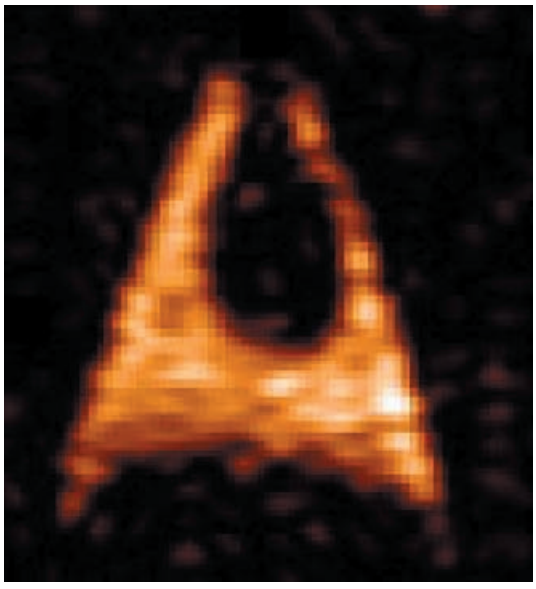

Fig. 3 Fluorine-19 MRI after inhalation of 80% sulfur hexafluoride gas in a pig showing homogeneous distribution of ventilation within both lungs

tion with oxygen enhancement, high signal visualization of the pulmonary tissue water and blood has been achieved as shown in Fig. 2. The image reflects the uptake of molecular oxygen from the air space into the pulmonary veins. Ventilation imaging simply by changing the inspiratory oxygen concentration is an attractive principle compared with nuclear medicine studies with inhalation of radioactive tracers. It does not require any special equipment or intravenous administration of exogenous agents. With appropriate postprocessing algorithms, it can be easily implemented into clinical routine, e.g., as a complementary step in the MR diagnosis of acute pulmonary embolism [16]. For the future, more studies are needed to evaluate the clinical value of this approach. Until now, it is unclear whether the individual contribution of regional changes of ventilation, oxygen uptake, or perfusion can be separated. The limitation of oxygen enhancement is its inability to perform dynamic imaging. To obtain sufficient contrast-to-noise ratio, multiple acquisitions are needed including the risk of motion artifacts; thus, motion correction algorithms are to be implemented.

Fluorine compounds

Compounds containing a relatively large number of fluorine (F)-19 atoms per molecule can be used as gaseous or liquid contrast agents for ventilation F-19 MRI (Larmor frequency 59.9 MHz). The low spin density of the intrapulmonary gas mixture is compensated by using either a high number of signal averages [17, 18] or by increasing the spin density by filling in a fluid compatible with gas exchange [19]. Inert fluorinated gases, such as tetrafluoromethane (CF4), hexafluoroethane (C2F6), or sulfur hexafluoride (SF6), possess a T1 time of the order of milliseconds [17]. The spin-rotation relaxation of these paramagnetic gases is so fast that the paramagnetism of oxygen has no effect. This short T1 makes rapid repetition radiofrequency pulses feasible. Together with a high number of signal averages, they compensate for the low spin density of the gas. Sulfur hexafluoride gas has the advantage that it is almost insoluble in blood, has no known toxic effect, is inexpensive, and has been used for many years in clinical trials as part of the multiple inert gas elimination technique. The drawbacks are that SF6 is not yet certified for clinical routine, and because of the higher density in comparison with the physiologically inhaled gases (O2, N2, CO2) transfer of data under normal ventilation conditions might be critical when compared with breathing ambient air. The first application of F-19 ventilation MRI using SF6 in an animal experiment with a scan time of 30 min was reported in 2000 [20]. The static approach for estimation of the ventilation–perfusion ratio in an animal model with partially obstructed left bronchi was achieved by measuring the ratio of the signal intensity using SF6 in combination with high and low O2 concentration. Imaging within a single breathhold becomes feasible by the use of ultrafast gradient-echo sequences [18, 21]. Image stacks with a spatial res-

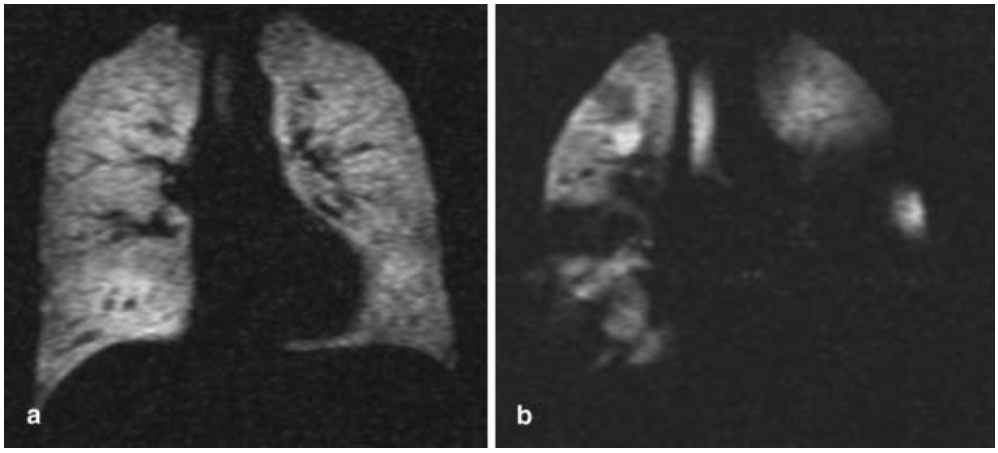

Fig. 4a, b Spin-density He-3 MRI after inhalation of hyperpolarized He-3 gas. **a** A 31-year-old healthy man showing homogeneous ventilation. **b** A 57-year-old man with bronchiolitis obliterans syndrome after right lung transplantation for emphysema showing multiple ventilation defects preferentially in the basal lung regions

olution of 4.7×6.3×15 mm^3 can be obtained during a breathhold of 49 s demonstrating homogeneous distribution of SF6 within porcine lungs (Fig. 3). For human applications, using an increased voxel size and a 2D gradient-echo sequence, dynamic imaging with a temporal resolution of 9.1 s becomes possible [21]. This technique can be used to determine wash-in and wash-out kinetics of SF6 non-invasively. This new method holds promise to measure more sophisticated physiological parameters such as residual volume or different pulmonary time constants.

Perfluorcarbon compounds (PFCs) have received increased interest in the past two decades for liquid ventilation because of their chemical inertness and their high solubility for oxygen and carbon dioxide. Liquid ventilation using PFC has been investigated as a new therapeutic strategy for the treatment of acute respiratory distress syndrome (ARDS). It eliminates surface tension related to pulmonary air/fluid interfaces, and improves pulmonary gas exchange in ARDS-associated surfactant depletion. Since the T1 of F-19 shows a linear dependency on the surrounding oxygen partial pressure, it can be used as a potential means to measure local pO2 in vivo [19, 22].

Hyperpolarized noble gases

Utilizing hyperpolarized noble gases with MRI is a recent approach for ventilation imaging. In 1994, Albert et al. demonstrated the possibility of imaging lung tissue filled with hyperpolarized xenon (Xe)-129 using MRI [23]. Helium-3 (He) was used in later studies because it has a much greater magnetic moment than Xe-129 and depolarizes more slowly. Helium-3 can be inhaled in relatively large quantities without substantial risks because it has no known toxic side effects and is not absorbed by the lung tissue. Xenon-129 compared with He-3 is much cheaper because He-3 is a very rare isotope, which is a by-product of tritium [hydrogen-3 (H-3)] decay. Two techniques for generating hyperpolarization have been established. The current techniques for He-3 yield polarization rates of 30–40% using spin exchange [24] and 35–50% using metastability exchange [25], whereas for Xe-129 it is only 5–7% [26]. The reader is referred to detailed reviews and original articles in the literature about these techniques [9, 27, 28, 29]. Recent success with hyperpolarized noble gas imaging has taken place with a standard 1.5-T MR scanner. Since the polarization is generated by optical pumping rather than by the magnetic field of the MR scanner, high-quality imaging in an open low field is possible with lower costs and more comfort for dyspneic patients [30].

Helium-3 MRI

Spin density

The morphological images are termed spin density or gas density because no special weightings or breathing techniques are used. The images reflect the gas-filled lung parenchyma with the potential to image the acinar units of the lung. The first studies showed excellent quality and resolution, which have a considerable potential for improved diagnosis of a variety of lung diseases such as emphysema and chronic obstructive pulmonary disease (COPD). Initial efforts were focused on visualizing He-3 in the lung during a breathhold. Because of the irreversible loss of the non-equilibrium polarization, careful consideration of image sequences and parameters is indispensable. A typical image series using He-3 acquiring approximately ten coronal images covering the whole lung requires a breathhold period of <10 s. Spatial resolution is significantly better than in nuclear medicine (2.5×2.5×10 mm). The data can also be used to measure the volume of the ventilated airspaces, revealing a good correlation (r=0.88) with the results of pulmonary func-

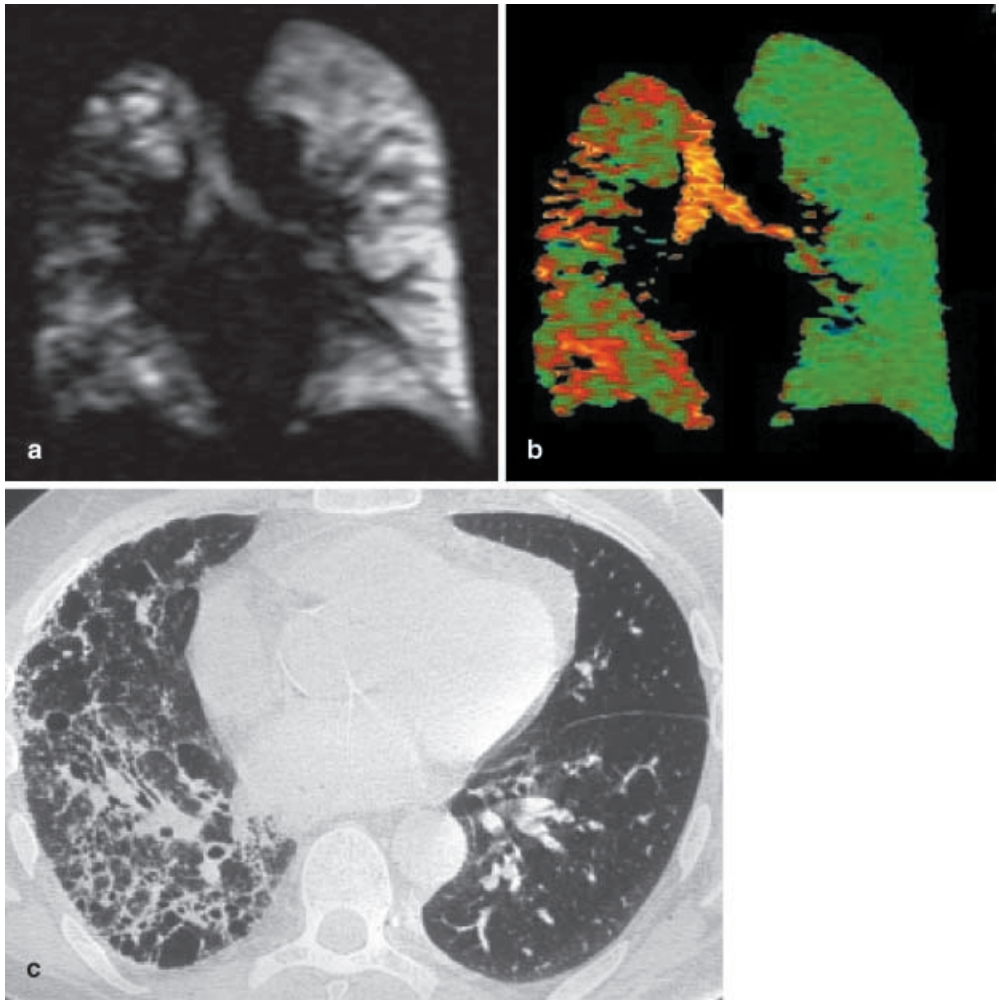

Fig. 5a–c Diffusion He-3 MRI after inhalation of hyperpolarized He-3 gas in a 62-year-old man after single lung transplantation on the left for fibrosis. **a** The diffusion-weighted image shows homogeneous signal in the transplanted, i.e., normal, left lung and inhomogeneous distribution in the native, i.e., fibrotic right lung. **b** The color-coded apparent diffusion coefficient map shows normal values and a homogeneous distribution on the left, and increased values with a heterogeneous distribution on the right. **c** Corresponding CT showing a normal transplanted left lung and a fibrotic right lung

tion tests (PFTs) [31]. Absolute lung volumes can be estimated after introduction of additional correction factors. Normal ventilation is represented by an almost complete and homogeneous distribution of He-3 signal within the lung (Fig. 4a) [32]. Some small (2 cm) transient ventilation defects in the gravity dependent regions of the lungs can be appreciated in healthy non-smokers [33]. They are caused by posture and the weight of the lung. In clinically healthy smokers, markedly more small ventilation defects can be depicted by He-3 MRI. They are thought to correspond to chronic inflammation and obstruction of small airways caused by smoking [25]. With FEV1 being normal, He-3 MRI demonstrates potentially reversible airways disease at an early stage.

Generally, circumscriptive ventilation defects, which are characterized by reduced signal intensity or complete lack of signal, are regarded as pathological findings. In asthma, reversible obstruction of the small airways results in impaired pulmonary ventilation. Associated ventilation defects are pleural based, frequently wedge shaped, and variable in size from tiny to segmental. In He-3 MRI mildly symptomatic asthmatics had larger and more numerous defects than asymptomatic asthmatics [33]. At follow-up, the mildly symptomatic asthmatics had multiple ventilation defects in different locations. Use of a bronchodilator in asymptomatic or mildly symptomatic asthmatic subjects partially or completely resolved the defects, even when the subject had inhaled a bronchoconstrictor before [33]; thus, He-3 MRI has the potential to be a sensitive test for assessing ventilation changes in the lung of asthmatic patients with normal PFTs and the response to therapy.

Helium-3 MRI also seems to be a good tool in diagnosis of chronic allograft rejection (bronchiolitis obliterans) in lung transplant recipients (Fig. 4b). Early diagnosis is of paramount importance for the introduction of adequate treatment to prevent long-term morbidity and mortality in patients after lung transplantation. Up to now, the early diagnosis is extremely difficult because changes are subtle at histological examination. In comparison with the established clinical grading system, scintigraphy, and CT scanning, He-3 MRI proved to be

more sensitive in the detection of ventilation defects in single- or double-lung transplant recipients [34]. McAdams et al. [35] found a correlation between the extent of ventilation defects at He-3 MRI and the severity of bronchiolitis obliterans. Further investigations showed preferential ventilation of the non-rejected transplant in comparison with the native lung by exhibiting a higher signal intensity [36].

Diffusion

A unique difference between conventional proton MRI and hyperpolarized gas imaging is the degree of "diffusive" Brownian motion. The diffusion coefficient of gases are 10^3–10^5 times greater than those of liquids. The interactions of the hyperpolarized gas atoms with the lung gases (N2, O2) and the restricted motion of the gas from the smaller length scales of the lung airspaces restrict the range for the diffusive motion, since the airspaces are of an order smaller than the unrestricted diffusion length of He-3. The restricted diffusive motion can be measured as the apparent diffusion coefficient (ADC) using specialized pulse sequences with a high magnetic field gradient to disrupt the signal following the same strength field gradient applied in the opposite direction to reconstitute the signal. If the molecules have moved between these pulses, the signal from that region will be attenuated (Fig. 5a). Using a series of diffusion-weighted images, an ADC map can be calculated (Fig. 5b).

First studies show diffusion maps of He-3 in healthy human lungs with uniformly distributed ADC values with typical mean values of 0.17–0.28 cm^2/s [37, 38, 39]. At expiration, an antero-posterior gradient of the ADC values becomes apparent which was not obvious at inspiration [40]; however, older subjects had higher ADC values with a larger standard deviation. These results are consistent with an increase in alveolar size, as a result of gradual loss of interstitial lung tissue, i.e., senile emphysema. In further studies ADC values were measured in patients with emphysema [39, 41, 42], COPD [43], and fibrosis (Fig. 5) [42]. The mean ADC values of these patients were found to be 2.5 times higher than in healthy volunteers indicating an increase of airspace size. Chronic obstructive pulmonary disease and emphysema patients showed a marked heterogeneity with a broadened histogram which was shifted towards higher ADC values as compared with healthy subjects. It has been demonstrated that the ADC is a useful indicator of the relative size of airspaces. It is a sensitive marker in the assessment of early emphysema [41] and other diseases that alter alveolar size as a result of alveolar wall destruction. With this new method it will be possible to perform studies to determine the normal aging pattern of the lung as well as to evaluate the long-term effect of drugs [44]. Very recent studies have already demonstrated that the sensitivity of the ADC measurement will be sufficient to detect early emphysematous changes [41].

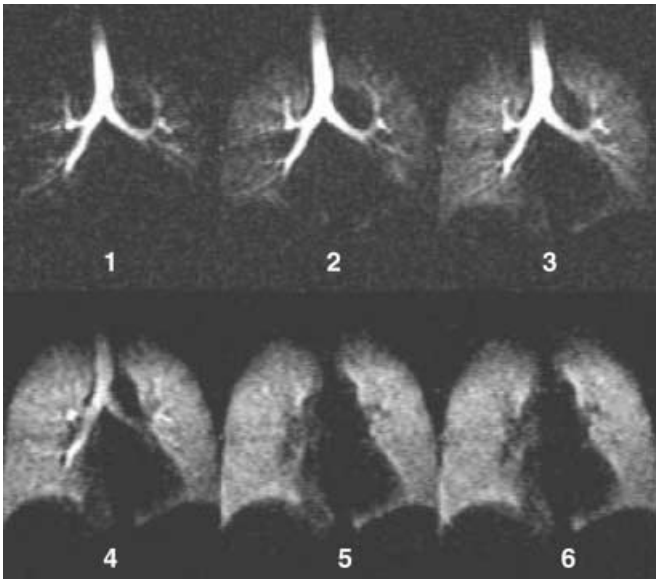

Fig. 6 Dynamic ventilation He-3 MRI after inhalation of hyperpolarized He-3 gas in a 27-year-old volunteer shows a rapid and homogeneous filling of the airspaces bilaterally

Dynamic ventilation

Another unique aspect of He-3 MRI is the possibility to visualize the distribution of ventilation during inspiration and expiration [45, 46, 47]. With the application of an optimized fast low-angle shot sequence imaging times of 130 ms on coronal projections were achieved (Fig. 6) [47]. The inflow of He-3 is very rapid. In volunteers, the signal appears almost simultaneously in the upper, middle and lower portions of the lung and a uniform wash-in and wash-out of the gas is observed [47]. With the application of single-shot echo-planar imaging three 10-mm axial slices can be measured with a temporal resolution of 122 ms simultaneously [48]. These axial slices demonstrated preferential ventilation of the posterior lung zones in supine position [46]. A significant improvement in the visualization of the distribution of ventilation was achieved by the development of a spiral sequence with image reconstruction using a sliding-window technique yielding a temporal resolution of 20 ms [49]. In contrast to the uniform pattern in volunteers diseased lungs are expected to exhibit a different, i.e. inhomogeneous, pattern of ventilation due to airway inflammation and differences in local compliance [49]. Thus, emphysema showed inhomogeneous sequential filling of airspaces with interspersed defects [46], redistribution while rebreathing, and prolonged washout, indicating air trap-

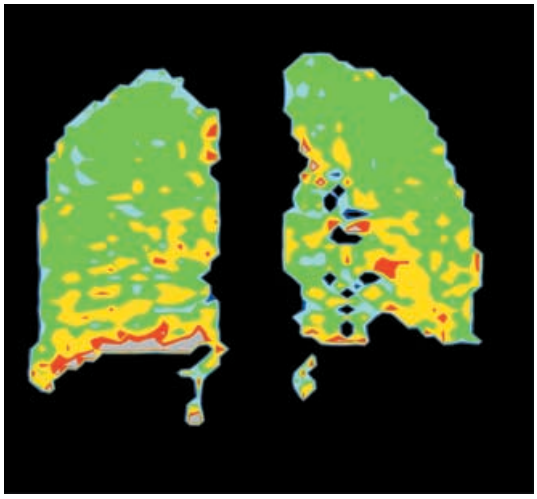

Fig. 7 Color-coded oxygen-sensitive He-3 MRI after inhalation of hyperpolarized He-3 gas in a 31-year-old male volunteer with a mean end-expiratory, i.e., alveolar, oxygen pressure of 127 mm Hg showing a homogeneous distribution with values of 100–160 mm Hg

ping, during expiration. For quantitative distribution analysis on a regional basis dedicated software tools, e.g. with motion correction, are under development [50]. These may further aid standardization of these measurements, which will be one of the requirements prior to introduction of this new technology into a clinical setting.

Oxygen measurement

Helium-3 MRI allows for regional and temporal analysis of intrapulmonary pO2 since the irreversible polarization loss of He-3 and the continual loss of signal are caused mainly by the radiofrequency pulses and relaxation due to paramagnetic molecular oxygen. These two effects can be separated by the application of two different imaging series using different intervals between image acquisitions [51]. The linear dependency between the concentration of oxygen and the T1 relaxation time of hyperpolarized He-3 is known from in vitro studies. It has been confirmed in live pigs correlating significantly (r=0.88) with global end-expiratory values from conventional respiratory gas analysis, which is an accepted way to measure alveolar pO2 [52]. It is important to realize that the knowledge of the alveolar pO2 also allows an estimation of regional pulmonary perfusion, which in addition to regional ventilation also determines alveolar pO2; thus, He-3 MRI is an attractive modality to visualize and quantify the ventilation/perfusion ratio on a regional basis (Fig. 7). In addition, oxygen uptake can be assessed. This potential has been confirmed in animal models with selective occlusion of pulmonary arteries. Inhomogeneous pO2 distribution was found in patients with emphysema and chronic pulmonary embolism indicating severe alterations of ventilation/perfusion matching [53].

Xenon-129 MRI

Besides He-3, Xe-129 can be imaged using MRI. In contrast to He-3, Xe-129 has a very high solubility in blood and lipid-rich tissue. Subsequently, dissolved-phase imaging becomes possible [54]. After administration by the inhaled route, Xe is absorbed into the pulmonary tissue and then enters the blood stream. From there it is distributed throughout the body by circulation. The resonance of Xe-129 is highly influenced by its surroundings inducing a chemical shift. In the dissolved phase the resonance of Xe-129 is shifted by approximately 200 ppm from the gas-phase resonance. As has been demonstrated in animal experiments (rats), chemical shift imaging in the lung, kidney, and brain becomes feasible [55, 56]. The resonances measured in humans and rats correspond to fat, tissue, and red blood cells. The collection of gas- and dissolved-phase signal is possible within a single acquisition resulting in a combined imaging and spectroscopic evaluation [54]. Combined visualization of the gas phase and dissolved phase by Xe-129 allows for simultaneous ventilation/perfusion studies. Studying the dynamics of the Xe-129 signal in the dog chest reveals even more insights into the uptake of Xe-129 [26]. After inhalation, the signal from tissue (or red blood cells) was destroyed by a selective gradient pulse. The signal decay in the gas phase was observed over time, providing a measure to characterize the absorption of Xe-129 into the tissue. Time constants of 61 ms were measured for tissue saturation with Xe-129 and 70 ms for red blood cell saturation. In analogy to Xe-CT, it can be postulated that the Xe can be used to perform perfusion studies of the brain (and possibly the heart), although additional technical adaptations will be required.

Conclusion

Magnetic resonance imaging of lung ventilation has made huge advances over the past years. It has opened pathways in animal research and the elucidation of basic pulmonary and airway pathophysiology. From there, it will almost certainly make its way into routine clinical applications. Without the need for using harmful ionizing radiation, MRI extends the principles of functional imaging from the central nervous system to the lung. It can be easily applied for repeated studies during follow-up as well as in the pediatric population. The novel strategies based on proton MRI, such as aerosolized gadolinium chelates and oxygen enhancement, are complement-

ed by non-proton MRI approaches. With the exception of hyperpolarized noble gases, these techniques are easy to implement, inexpensive, and very likely useful in ventilation imaging. On the other hand, hyperpolarized He-3 MRI offers superior SNR, as well as high spatial and temporal resolution opening an immense field of experimental approaches, to acquire regional information on lung morphology and pulmonary function, which have remained uncharted by the techniques available until now. Attempts are being made to enhance the availability of hyperpolarized He-3 gas, which will allow further implementation and dissemination into an increasing number of centers.

Acknowledgements We gratefully acknowledge the support of the He-3 projects in Mainz and Sheffield by the German Research Council (DFG), the Max Planck Society (MPG), the European Commission ("COPHIT" and "PHIL"), the Engineering and Physical Sciences Research Council (EPSRC), the British Council together with the German Academic Exchange Program (DAAD), and Amersham Health.

References

1. Kramer SS, Hoffman EA (1995) Physiologic imaging of the lung with volumetric high-resolution CT. J Thorac Imaging 10:280–290
2. Kauczor H-U, Hast J, Heussel C, Schlegel J, Mildenberger P, Thelen M (2000) Focal airtrapping at expiratory high-resolution CT: comparison with pulmonary function tests. Eur Radiol 10:1539–1546
3. Markstaller K, Arnold M, Döbrich M, Karmrodt J, Weiler N, Uthmann T, Eberle B, Thelen M, Kauczor H-U (2001) A software tool for automatic image-based ventilation analysis using dynamic chest CT-scanning in healthy and ARDS lungs. Fortschr Röntgenstr 173:830–835
4. Simon B, Marcucci C, Fung M, Lele S (1998) Parameter estimation and confidence intervals for Xe-CT ventilation studies: a Monte Carlo approach. J Appl Physiol 84:709–716
5. Thiele J, Klöppel R (1995) Computertomographische Messung der Lungenventilation durch Inhalation von Isovist 300. Röntgenpraxis 48:259–260
6. White P, Hayward M, Cooper T (1991) Ventilation agents: What agents are currently used? Nucl Med Commun 12:349–352
7. Nagao M, Murase K, Ichiki T, Sakai S, Yasuhara Y, Ikezoe J (2000) Quantitative analysis of technegas SPECT: evaluation of regional severity of emphysema. J Nucl Med 41:590–595
8. Schuster D (1998) The evaluation of lung function with PET. Semin Nucl Med 28:341–351
9. Kauczor H-U, Surkau R, Roberts T (1998) MRI using hyperpolarized noble gases. Eur Radiol 8:820–827
10. Montgomery A, Paajanen H, Brasch R, Murray J (1987) Aerosolized gadolinium-DTPA enhances the magnetic resonance signal of extravascular lung water. Invest Radiol 22:377–381
11. Misselwitz B, Muhler A, Heinzelmann I, Bock J, Weinmann H (1997) Magnetic resonance imaging of pulmonary ventilation. Initial experiences with a gadolinium-DTPA-based aerosol. Invest Radiol 32:797–801
12. Haage P, Adam G, Pfeffer J, Tacke J, Karaagac S, Barker M, Guenther R (2000) Demonstration of pulmonary ventilation in MR imaging of the lung: initial results with a gadolinium-DTPA aerosol. Fortschr Roentgenstr 172:323–328
13. Edelman R, Hatabu H, Tadamura E, Lei W, Prasad P (1996) Noninvasive assessment of regional ventilation in the human lung using oxygen-enhanced magnetic resonance imaging. Nature Med 2:1236–1239
14. Löffler R, Mueller C, Peller M, Penzkofer H, Deimling M, Schwabelmaier M, Scheidler J, Reiser M (2000) Optimization and evaluation of the signal intensity change in multisection oxygen-enhanced MR lung imaging. Magn Reson Med 43:860–866
15. Mai V, Chen Q, Bankier A, Edelman R (2000) Multiple inversion recovery MR subtraction imaging of human ventilation from inhalation of room air and pure oxygen. Magn Reson Med 43:913–916
16. Chen Q, Levin D, Kim D, David V, McNicholas M, Chen V, Jakob P, Griswold M, Goldfarb J, Hatabu H, Edelman R (1999) Pulmonary disorders: ventilation–perfusion MR imaging with animal models. Radiology 213:871–879
17. Kuethe DO, Caprihan A, Fukushima E, Waggoner RA (1998) Imaging lungs using inert fluorinated gases. Magn Reson Med 39:85–88
18. Schreiber W, Markstaller K, Weiler N, Eberle B, Laukemper-Ostendorf S, Scholz A, Bürger K, Thelen M, Kauczor H-U (2000) 19F-MRT der Lungenventilation in Atemanhalteantechnik mittels SF6 Gas. Fortschr Roentgenstr 172:500–503
19. Laukemper-Ostendorf S, Scholz A, Bürger K, Heussel CP et al. (2002) 19F-MRI of perflubron for measurement of oxygen partial pressure in porcine lungs during partial liquid ventilation. Magn Reson Med 47:82–89
20. Kuethe DO, Caprihan A, Gach HM, Lowe IL, Fukushima E (2000) Imaging of obstructed ventilation with NMR using inert fluorinated gases. J Appl Physiol 88:2279–2286
21. Schreiber W, Weiler N, Markstaller K, Eberle B, Scholz A, Bürger K, Thelen M, Kauczor H-U (2001) Dynamic 19F-MRI of sulfur hexafluoride (SF6) gas in the lung. Magn Reson Med 45:605–613
22. Heussel C, Scholz A, Schmittner M, Laukemper-Ostendorf S et al. (2001) To elucidate the physiology of liquid ventilation: measurements of alveolar pO2 using ^{19}F-MRI. Proc Intl Soc Mag Reson Med 9:184
23. Albert MS, Cates GD, Driehuys B, Happer W, Saam B, Springer SR, Wishnia A (1994) Biological magnetic resonance imaging using laser-polarized 129 Xe. Nature 370:199–201
24. DeLange E, Mugler J, Brookeman J, Knight-Scott J, Truwit J, Teates C, Daniel T, Bogorad P, Cates G (1999) Lung airspaces: MR imaging evaluation with hyperpolarized He gas. Radiology 210:851–857
25. Guenther D, Eberle B, Hast J, Lill J et al. (2000) 3He MRI in healthy volunteers: preliminary correlation with smoking history and lung volumes. NMR Biomed 13:182–189
26. Ruppert K, Brookeman J, Hagspiel K, Driehuys B, Mugler J (2000) NMR of hyperpolarizd Xe-129 in the canine chest: spectral dynamics during a breath-hold. NMR Biomed 13:220–228
27. Guenther D, Hanisch G, Kauczor H-U (2000) Functional magnetic resonance imaging of pulmonary ventilation using hyperpolarized noble gases. Acta Radiol 41:519–528

28. Kauczor H-U, Chen X, Beek E van, Schreiber W (2001) Pulmonary ventilation imaged by magnetic resonance: at the doorstep of clinical application. Eur Respir J 17:1–16
29. Möller HE, Chen XJ, Saam B, Hagspiel KD, Johnson GA, Altes TA, Lange EE de, Kauczor H-U (2002) MRI of the lungs using hyperpolarized noble gases. Magn Reson Med DOI 10.1002/mrm.10173
30. Darrasse L, Guillot G, Nacher P-J, Tastevin G (1997) Low-field 3He nuclear magnetic resonance in human lungs. CR Acad Sci Paris 324:691–700
31. Kauczor H-U, Markstaller K, Puderbach M, Lill J, Eberle B, Hanisch G, Grossmann T, Heussel C, Schreiber W, Thelen M (2001) Volumetry of ventilated airspaces using 3He MRI: preliminary results. Invest Radiol 36:110–114
32. Kauczor H-U, Ebert M, Kreitner K-F, Nilgens H, Surkau R, Heil W, Hofmann D, Otten E, Thelen M (1997) Imaging of the lungs using 3He MRI: preliminary clinical experience. J Magn Reson Imaging 7:538–543
33. Altes T, Powers P, Knight-Scott J, Rakes G, Platts-Mills T, deLange E, Alford B III, Brookeman J (2001) Hyperpolarized 3He MR lung ventilation imaging in asthmatics: preliminary findings. J Magn Reson Imaging 13:378–384
34. Gast K, Viallon M, Eberle B, Lill J, Puderbach M, Hanke A, Schmiedeskamp J, Kauczor H-U (2002) MRI in lung transplant recipients using hyperpolarized ^{3}He: comparison with CT. J Magn Reson Imaging 15:268–274
35. McAdams H, Palmer SM, Donnelly L, Charles H, Tapson V, MacFall J (1999) Hyperpolarized 3He-enhanced MR imaging of lung transplant recipients: preliminary results. Am J Roentgenol 173:955–959
36. Kauczor H-U, Eberle B, Lill J, Schreiber W, Hanisch G, Markstaller K, Günther D, Diergarten T, Weiler N (2000) Funktionelle Strategien zur Untersuchung der Ventilation bei einseitig Lungentransplantierten mittels He-3 MRT. Fortschr Röntgenstr 172:S16
37. Mugler J, Brookeman J, Knight-Scott J, Maier T, de Lange E, Bogorad P (1998) Regional measurement of the 3He diffusion coefficient in the human lung. Proc Int Soc Mag Reson Med 6:1906
38. Schreiber W, Markstaller K, Eberle B, Kauczor H-U, Hanisch G, Weiler N, Surkau R, Thelen M (1999) Ultrafast MRI of 3D distribution of hyperpolarized helium-3 diffusion coefficient in the lung. Eur Radiol 9:S542
39. Saam B, Yablonskiy D, Kodibagkar V, Leawoods J, Gierada D, Cooper J, Lefrak S, Conradi M (2000) MR imaging of diffusion of 3He gas in healthy and diseased lungs. Magn Reson Med 44:174–179
40. Bink A, Hanisch G, Lill J, Schreiber W, Thelen M, Kauczor H (2001) The apparent diffusion coefficient at 3He MRI: analysis of airspace size at in- and expiration. Radiology 221:P631
41. Salerno M, de Lange E, Altes T, Truwit J, Brookeman J, Mugler J (2002) Emphysema: hyperpolarized helium-3 diffusion MR imaging of the lungs compared with spirometric indexes: initial experience. Radiology 222:252–260
42. Bink A, Gast K, Hanisch G, Lill J, Vogel A, Mayer E, Schreiber W, Thelen M, Kauczor H-U (2001) Analysis of airspace size in healthy volunteers and single lung transplant recipients using the apparent diffusion coefficient at 3He-MRI. Eur Radiol 11:S214
43. Salerno M, Brookeman J, de Lange E, Knight-Scott J, Mugler J (2000) Detection of regional microstructural changes of the lung in emphysema using hyperpolarized 3 He diffusion MRI. Proc Int Soc Mag Reson Med 8:9
44. Leawoods J, Yablonskiy D, Gierada D, Conradi M (2001) Ventilation abnormalities and diffusion coefficients in the lung of asymptomatic smokers. Proc Int Soc Mag Reson Med 9:185
45. MacFall J, Charles H, Black R, Middleton H et al. (1996) Human lung airspaces: potential for MR imaging with hyperpolarized He-3. Radiology 200:553–558
46. Gierada D, Saam B, Yablonskiy D, Cooper J, Lefrak S, Conradi M (2000) Dynamic echo planar MR imaging of lung ventilation with hyperpolarized He-3 in normal subjects and patients with severe emphysema. NMR Biomed 13:176–181
47. Schreiber W, Weiler N, Kauczor H-U, Markstaller K et al. (2000) Ultraschnelle MRT der Lungenventilation mittels hochpolarisiertem Helium-3. Fortschr Röntgenstr 172:129–133
48. Saam B, Yablonskiy DA, Gierada DS, Conradi MS (1999) Rapid imaging of hyperpolarized gas using EPI. Magn Reson Med 42:507–514
49. Salerno M, Altes T, Brookeman J, deLange E, Mugler J (2001) Dynamic spiral MRI of pulmonary gas flow using hyperpolarized 3He: preliminary studies in healthy and diseased lungs. Magn Reson Med 46:667–677
50. Gast K, Puderbach MU, Rodriguez I, Eberle B, Markstaller K, Hanke AT, Schmiedeskamp J, Weiler N, Lill J, Schreiber WG, Thelen M, Kauczor H-U (2002) Dynamic ventilation ^{3}He-MRI with lung motion correction: gas flow distribution analysis. Invest Radiol 37:126–134
51. Deninger A, Eberle B, Ebert M, Grossmann T et al. (1999) Quantitation of regional intrapulmonary oxygen partial pressure evaluation during apnoe by 3He-MRI. J Magn Reson 141:207–216
52. Eberle B, Weiler N, Markstaller K, Kauczor H-U et al. (1999) Analysis of regional intrapulmonary O2-concentrations by MR imaging of inhaled hyperpolarized helium-3. J Appl Physiol 87:2043–2052
53. Eberle B, Weiler N, Markstaller K, Kauczor H-U, Deninger A, Schreiber W, Dick W (1999) Determination of regional intrapulmonary oxygen concentration by magnetic resonance imaging of inhaled hyperpolarized 3Helium. Crit Care Med 27:A162
54. Mugler JP, Driehuys B, Brookeman JR, Cates GD et al. (1997) MR imaging and spectroscopy using hyperpolarized 129Xe gas: preliminary human results. Magn Reson Med 37:809–815
55. Swanson S, Rosen M, Agranoff B, Coulter K, Welsh R, Chupp T (1997) Brain MRI with laser-polarized Xe-129. Magn Reson Med 38:695–698
56. Swanson S, Rosen M, Coulter K, Welsh R, Chupp T (1999) Distribution and dynamics of laser-polarized 129Xe magnetization in vivo. Magn Reson Med 42:1137–1145